Radiative recombination of large polarons in halide perovskites

Mingliang Zhang[1,2], Xu Zhang[2], Hai-Qing Lin[1] and Gang Lu[2]

[1] Beijing Computational Science Research Center, Beijing 100193, People's Republic of China
[2] Department of Physics and Astronomy, California State University Northridge, Northridge, CA 91330, United States of America

E-mail: ganglu@csun.edu

Abstract
In hybrid organic/inorganic perovskites, the majority of charge carriers are large polarons. Slow recombination of the large polarons underlies long carrier lifetime and diffusion length, crucial to optoelectronic applications of the perovskites. However, microscopic mechanisms by which the large polarons recombine remain largely unknown. Here we propose a theoretical model to elucidate radiative recombination of large polarons. Six annihilation pathways are identified which involve the formation of mobile and immobile 'dying pairs', both responsible for charge recombination. The formation probability of the 'dying pair' and the corresponding annihilation rate can be estimated. The product of the formation probability and the annihilate rate gives rise to recombination rate along each pathway and weighted sum of the recombination rates yields an overall rate of radiative recombination in perovskites. The theory sheds light on the physical mechanism by which large polarons recombine via the formation of the dying pairs, assisted by thermal activation and quantum tunneling. The predictions from the theory in general agree well to corresponding experimental measurements on monomolecular and bimolecular recombination rates as well as peak frequency of photoluminescence spectrum.

Keywords: polaron, radiative recombination, dying pair, photoluminescence spectra

S Supplementary material for this article is available online

(Some figures may appear in colour only in the online journal)

1. Introduction

Organic–inorganic halide perovskites (OIHPs) have recently emerged as highly efficient and promising optoelectronic materials with potential applications in photovoltaics, light-emitting diodes and low-threshold lasers [1–3]. The exceptional optoelectronic performance of OIHPs has been attributed to their high optical absorption coefficients, low exciton binding energies, long carrier lifetime and diffusion lengths. In particular, slow radiative recombination rates coupled with high fluorescent yield and wavelength tunability render OIHPs particularly attractive for photovoltaic and lasing applications.

The OIHPs are soft and polar, with large and long-range electron–phonon coupling, leading to the formation of polarons. It has been proposed that dominant charge carriers in OIHPs are large polarons, formed by the interaction between electrons (or holes) with longitudinal optical (LO) phonons [4, 5]. The formation of large polarons underpins some of the key characteristics of OIHPs, including (i) inverse power law temperature dependence of charge carrier mobility ($\mu \propto T^{-3/2}$) [4, 6–8]—a signature of coherent transport scattered by longitudinal acoustic (LA) phonons, (ii) long carrier diffusion length and lifetime [4, 5, 9–12], and (iii) exceptionally low scattering rates for hot carriers [6, 13, 14]. In particular, the formation of large polarons provides scenarios in which the charge carriers are protected from scattering with charged defects, LO phonons and each other. It should be noted that the electron and hole polarons have been theoretically investigated in related ABO_3 perovskites [15, 16].

1

In addition, the valence band structures of the halide perovskites (e.g. MAPbBr$_3$ [17, 18] and MAPbI$_3$ [19]) have recently been measured by angle-resolved photoemission spectroscopy (ARPES), based on which one can estimate the effective mass of charge carriers. As the valence band maximum is most representative of the holes under low carrier concentrations, we can calculate the effective mass at the M-point of the Brillouin zone [17] in MAPbBr$_3$ as $m^* \sim 1.8$ m (m is the mass of free electron). Following the classical theory of large polarons [20], one can also estimate [7] the effective mass $m^* \sim 4$ m of a large polaron in MAPbBr$_3$ using its static ($\varepsilon_0 = 70$) and optical dielectric constants ($\varepsilon_\infty = 6.5$) [21]; this value is in the same order of magnitude as that estimated from the ARPES experiments. In contrast, the effective mass of a free hole was estimated as $m^* \sim 0.2$ m from first-principles band structure calculations [9, 22], which is much smaller than the ARPES value. Thus, the ARPES data suggests that the dominant charge carriers in hybrid halide perovskites are likely large polarons, as opposed to free carriers. It is also important to clarify that the large polaron model can indeed explain $\mu \propto T^{-3/2}$ dependence by realizing that the residual interaction between the polaron and the optical phonons is much weaker than the interaction between the polaron and the acoustic phonons [7]. The original Frohlich model failed to explain the temperature dependence [10, 12] because it ignored the interaction between the polaron and the acoustic phonons, which is important in OIHPs [4, 5, 7]. Although further experiments are needed to ascertain the nature of charge carriers (large polarons versus free carriers), it's reasonable to believe that large polarons play important roles in charge transport and charge recombination of the OIHPs. Finally, the existence of large polarons in OIHPs has also received support from density functional theory calculations [23].

Despite its conceptual importance, the large polaron picture has not been widely utilized to provide quantitative analysis of optoelectronic properties in OIHPs, with the exception of the work by Emin [24] and by Munson *et al* [25]. For instance, although the interaction energy between two oppositely charged large polarons—an electron polaron (EP) and a hole polaron (HP)—as a function of their distance has been worked out recently [24], it is not clear how would two large polarons recombine in OIHPs. In addition, there is no microscopic theory that can predict recombination dynamics of large polarons in relevant temperature range, i.e. 0–400 K (with the low temperature in laser and room temperature for photovoltaic applications). Note that the typical timescale for radiative charge recombination is 10^{-9} s in MAPbI$_3$ [26]. The timescale for polaron formation, on the other hand, can be estimated by the vibrational frequencies of the LO phonons (e.g. Pb–I stretching and I–Pb–I bending modes) in MAPbI$_3$, which are around 10^{-13}–10^{-12} s [14]. Thus, the formation of large polarons proceeds much faster than their annihilation, hence the study of their recombination is relevant in OIHPs. Additionally, in working conditions of solar cells, light-emitting diodes and lasers, light absorption and radiative recombination are not in equilibrium with each other. Thus the detailed balance does not apply and a strong absorption does not imply a slow recombination [27, 28]. It is amply
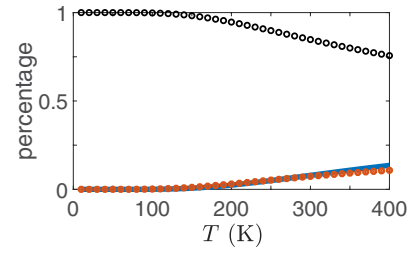

Figure 1. The percentage of polarons (open circle), excitons (filled circle) and free carriers (blue solid line) as a function of temperature T.
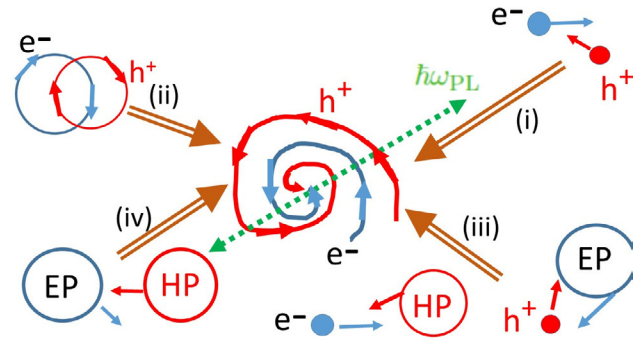

Figure 2. Pictorial diagram of the pathways (i)–(iv). A single line arrow represents a collision between two particles and a double line arrow represents the formation of a mobile dying pair after the collision; a dashed line represents the annihilation of the mobile dying pair and the radiation of a photon with frequency $\hbar\omega_{PL}$.

clear that a fundamental theory on radiative recombination of large polarons is necessary and in fact, highly desirable for the future development of OIHPs. In this paper, we propose a theoretical model that elucidates the fundamental processes underlying the recombination of large polarons in OIHPs, and provides quantitative analysis of recombination dynamics. As the application of the theory, we estimate the monomolecular and bimolecular charge recombination rates as well as peak frequency of photoluminescence (PL) spectrum at different temperatures, all of which compare well to experimental results.

2. Statistical weights of six pathways for radiative recombination

In an OIHP single crystal, the photo-generated carrier concentration (10^{13}–10^{19} cm^{-3}) is much larger than the concentration of deep defect states ($<10^{11}$ cm^{-3}) [29, 30]. Thus, the majority of the photo-generated carriers exist as electron (hole) polarons, excitons, free electrons (holes), and shallow trapped carriers. There are six pathways contributing to the monomolecular and bimolecular recombinations: (i) two free mobile carriers; (ii) an electron–hole pair in an exciton; (iii) a free carrier and a large polaron; (iv) two large polarons; (v) one free mobile carrier and one trapped 'free' carrier; and (vi) a trapped 'free' carrier and a large polaron. Each pathway could contribute to the overall recombination with a statistical weight, denoted by p_{2f}, p_{ex}, p_{Pf}, p_{2P}, p_{ft}, p_{Pt}, respectively.
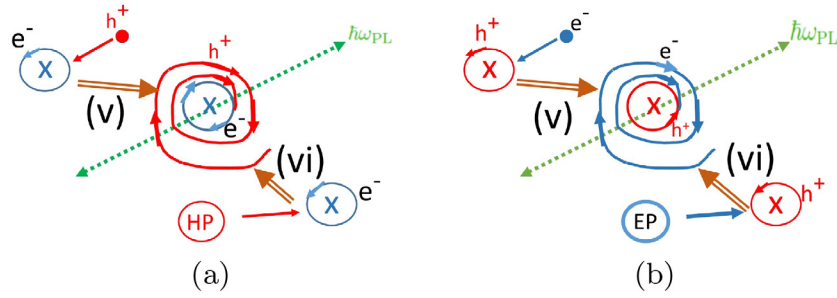
Figure 3. Pictorial diagram of the pathways (v) and (vi). A single line arrow represents a collision between two particles and a double line arrow represents the formation of an immobile dying pair after the collision; a dashed line represents the annihilation of the immobile dying pair and the radiation of a photon with frequency $\hbar\omega_{\mathrm{PL}}$.

Most trap centers in OIHPs are charged with a trapping energy between $k_{\mathrm{B}}T$ and 0.2 eV [31, 32] and thus are mainly responsible for radiative as opposed to non-radiative recombination. Here we will focus on these charged and moderately shallow trap centers. The pathways (i), (iii) and (iv) contribute to the bimolecular recombination while the pathways (ii), (v) and (vi) contribute to the monomolecular recombination.

Since radiative recombination is slower ($>10^{-9}$ s) than the dissociation and formation of excitons ($\sim 10^{-15}$ s) and polarons ($\sim 10^{-12}$ s), we assume that the free carriers (electrons or holes), excitons and polarons are in thermal equilibrium with each other at temperature T. Hence, the percentage of electrons (or holes) is $p_{\mathrm{f}} = f_{\mathrm{f}}^0 + f_{\mathrm{ex}}^0 e^{-E_{\mathrm{ex}}/k_{\mathrm{B}}T} + f_{\mathrm{P}}^0 e^{-F_{\mathrm{P}}/k_{\mathrm{B}}T}$, where k_{B} is Boltzmann constant; E_{ex} is the exciton binding energy; $F_{\mathrm{P}}(T)$ is the formation free energy of polaron [7], $f_{\mathrm{f}}^0 = [1 + e^{E_{\mathrm{ex}}/k_{\mathrm{B}}T} + e^{F_{\mathrm{P}}/k_{\mathrm{B}}T}]^{-1}$, $f_{\mathrm{ex}}^0 = e^{E_{\mathrm{ex}}/k_{\mathrm{B}}T} f_{\mathrm{f}}^0$, and $f_{\mathrm{P}}^0 = e^{F_{\mathrm{P}}/k_{\mathrm{B}}T} f_{\mathrm{f}}^0$. The percentage of excitons is given by $p_{\mathrm{ex}} = f_{\mathrm{ex}}^0 (1 - e^{-E_{\mathrm{ex}}/k_{\mathrm{B}}T})$ and the percentage of polarons is $p_{\mathrm{P}} = f_{\mathrm{P}}^0 (1 - e^{-F_{\mathrm{P}}/k_{\mathrm{B}}T})$.

In MAPbI$_3$, $E_{\mathrm{ex}} \sim 16$ meV [33]. The formation free energy $F_{\mathrm{P}}(T)$ of polaron has been calculated in [7] from the formation energy E_{P} of polaron and change in entropy. In figure 1, we plot p_{f}, p_{ex} and p_{P} as a function of temperature. It is found that in the temperature range of 0–350 K, the percentage of polarons is larger than that of excitons and free carriers, and beyond 300 K, the percentage of the free carriers is slightly higher than that of the excitons.

The statistical weight of the four decay pathways (i)–(iv) concerning the mobile dying pairs is: $p_{2\mathrm{f}} = p_{\mathrm{f}}^2$, p_{ex}, $p_{\mathrm{Pf}} = p_{\mathrm{f}} p_{\mathrm{P}}$, and $p_{2\mathrm{P}} = p_{\mathrm{P}}^2$. Let E_{tra} be the trap energy defined relative to the edge of the valence (conduction) band for the hole (electron) [32], then the probability that a carrier is trapped is $1 - e^{-E_{\mathrm{tra}}/k_{\mathrm{B}}T}$. Thus the statistical weight of the pathways (v) and (vi) involving the immobile pairs is $p_{\mathrm{ft}} = p_{\mathrm{f}} (1 - e^{-E_{\mathrm{tra}}/k_{\mathrm{B}}T})$, and $p_{\mathrm{Pt}} = p_{\mathrm{P}} (1 - e^{-E_{\mathrm{tra}}/k_{\mathrm{B}}T})$.

3. Dying pair

Recombination probability of two oppositely charged carriers becomes significant only when there is overlap between their wave-functions. However, the typical radius of a large polaron in OIHP is a few nanometers [4, 5, 7], much greater than the overlapping distance of their wave-functions,

therefore the electron and the hole must break free from the surrounding lattice distortion in order to recombine radiatively. The escape of the carriers can be facilitated by thermal activation and/or quantum tunneling. It is thus convenient to define a critical distance (L) below which the dominant physical process is annihilation of the charge carriers; other competing processes, such as (re)formation of polarons and excitons can be neglected. In the following, we name the charge carriers escaped from their surrounding lattice distortion as 'free' carriers and the electron–hole pairs entering the critical distance as 'dying pairs'. Importantly, there are *only* two types of dying pairs in our theory: type I consists of two mobile free carriers, referred to mobile pairs in the paper, and type II consists of one mobile and one trapped 'free' carrier, referred to immobile pairs. Each type is associated with a unique critical distance and the dying pairs of the same type are considered indistinguishable. In other words, all mobile (or immobile) dying pairs are identical, and their electron–hole distances are immaterial in the theory. However, the mobile and immobile pairs could have distinct critical distances.

Along the pathways (i)–(iv), the electron and hole are not trapped. Once a dying pair is formed, it is mobile. As shown schematically in figure 2, each recombination process consists of a collision, the formation of a mobile dying pair and the eventual radiative annihilation. Along the pathways (v) and (vi), one of the two carriers is trapped and the corresponding dying pair is thus immobile. The schematic picture of the pathways (v) and (vi) are shown in figure 3. Note that for any charge recombination, each pathway proceeds simultaneously and independently.

Along each pathway, the dying pairs of the same type would form and annihilate at certain rates. Thanks to these simplifications, we can reduce the original problem to the formation of the dying pairs and their subsequent annihilation. Along each pathway, there is only one type of dying pairs. The recombination rate of each pathway is a product of the formation probability of the dying pair and its annihilation rate. By knowing the recombination rate and the statistical weight of each pathway, we can estimate the monomolecular and bimolecular charge recombination rates as well as the peak frequency of PL spectrum. Our microscopic theory is applicable to all ionic and polar semiconductors, in which primary charge carriers are large polarons. And once combined

with first-principles parameterization, the theory will also be predictive.

In the following, we provide an estimate of the critical distance—the most essential property of the dying pairs—in a prototypical OHIP, MAPbI$_3$. Because this distance is expected to be on the same order of the lattice constant, the hydrogenic model would be appropriate to describe the dying pairs. We denote the binding energy of the dying pair as B and it can be expressed as $B = m_r(Ke^2/\varepsilon\hbar)^2/2$. Here $K = (4\pi\epsilon_0)^{-1}$, ϵ_0 is permittivity in free space. m_r is the reduced mass of the dying pair and ε is the dielectric constant. By definition, the dying pair must be stable against thermal dissociation, formation of an exciton, and formation of two polarons. Therefore its binding energy must be greater than the thermal energy k_BT, exciton binding energy E_{ex} and formation free energy of a polaron pair ($2F_P$). Given the fact that only a few ions are within the critical distance, the ionic contribution to the dielectric screening can be neglected. As a result, the effective Coulomb attraction V_{eh} between the electron and hole of the dying pair can be approximated as $V_{eh} = V_{eh}^{bare}/\varepsilon_\infty$, where ε_∞ is the dielectric constant from the bound electrons and $V_{eh}^{bare} = -Ke^2/d_{eh}$ is the bare Coulomb interaction. Here d_{eh} is the distance between the electron and hole.

The effective mass of a quasi-particle is determined by its interaction with other particles in its vicinity. For the electron and the hole in a dying pair, the dominant interaction is the Coulomb attraction between them owing to their close distance. This interaction is much stronger than that between the electron (or the hole) with the nuclei. Thus, the effect of the band structure on the dying pair can be ignored, and the effective mass of the electron (and hole) in the dying pair can be approximated by that of a bare electron, m. In other words, for the mobile dying pair, we have $m_r^m = m/2$ and the binding energy $B_m = m(Ke^2/\varepsilon_\infty\hbar)^2/4$, and for the immobile pair, $m_r^i = m$ and $B_i = 2B_m$. The critical distance of the mobile dying pair can be calculated as $L_m = 2\varepsilon_\infty\hbar^2/(mKe^2)$, and for the immobile pair, $L_i = L_m/2$. In MAPbI$_3$, $\varepsilon_\infty = 6.5$ [34], thus $B_m = 162$ meV, $L_m = 6.8$ Å, and $L_i = 3.4$ Å. The exciton binding energy of MAPbI$_3$ is between 16–50 meV [33] and the maximum formation free energy of large polaron pairs is about 140 meV at $T = 0$ K and 124 meV at $T = 300$ K [7], both less than B_m and B_i. Therefore, we can establish the stability of the dying pairs whose critical distances are in the order of the lattice constant as expected.

4. The formation probability and annihilation rate of dying pairs

Next, we set out to estimate the recombination rate in each pathway via either the mobile or immobile dying pairs. To this end, we need to determine the annihilation rates of the mobile and immobile dying pairs, as well as their formation probability in each pathway. We first consider the annihilation of two free carriers, which are not necessarily a dying pair, and calculate their annihilation rate (or transition probability per unit time) w_{2f}. These carriers can move freely in the lattice and recombine with or without the assistance of phonons.

By approximating their wave-functions with planewaves, we can derive w_{2f} based on the second-order perturbation theory with the electron–phonon and electron–photon interactions treated as perturbations [26, 35, 36]:

$$w_{2f} = \frac{e^2}{V4\pi\epsilon_0} \frac{n_{cell}\hbar^2\omega_{\mathbf{k}}}{m^2c^3\omega_{\mathbf{q}}^g} \Big|\frac{\epsilon_{\mathbf{k}\sigma\beta}k_{3\beta}}{\varepsilon(\omega_{\mathbf{k}})}\Big|^2$$

$$\frac{n_{\mathbf{q}}^g}{[E_{c\mathbf{k}+\mathbf{k}_3} - E_{c\mathbf{k}_1} - \hbar\omega_{\mathbf{q}}^g]^2} \Big|\frac{e^{-i\mathbf{q}\cdot\mathbf{s}_\kappa}}{\sqrt{M_\kappa}} \frac{e_{\kappa\alpha}^g(\mathbf{q})q_\alpha z_\kappa e^2}{\epsilon_0 q^2\varepsilon(\omega_{\mathbf{q}}^g, T)}\Big|^2, \quad (1)$$

where the repeated indices are summed over; V is the volume of the sample; n_{cell} is the number of unit cells per volume; M_κ and z_κ are the mass and effective nuclear charge of the κth atomic core. $\mathbf{s}_\kappa$ is the position vector of the κ th atom relative to the center of the primitive cell. $\mathbf{k}$ and $\omega_{\mathbf{k}}$ are the wave vector and frequency of emitted photon. $\varepsilon(\omega_{\mathbf{k}})$ is the dielectric constant at PL frequency $\omega_{\mathbf{k}}$. $\epsilon_{\mathbf{k}\sigma\beta}$ is the βth Cartesian component of the σth polarization vector of photon. $\mathbf{k}_1$ is the electron wave vector in the conduction band, and $E_{c\mathbf{k}_1}$ is the energy of the electron in a state $|c\mathbf{k}_1\rangle$ of the conduction band c. $\mathbf{k}_3$ is the wave vector of the hole in the valence band. $\mathbf{q} = \mathbf{k} + \mathbf{k}_3 - \mathbf{k}_1$ is the phonon wave vector and g is the phonon branch index. $\omega_{\mathbf{q}}^g$ and $n_{\mathbf{q}}^g$ are the frequency and occupation number of the phonon in mode $|g\mathbf{q}\rangle$, $\varepsilon(\omega_{\mathbf{q}}^g, T)$ is the dielectric constant at the phonon frequency $\omega_{\mathbf{q}}^g$. w_{2f} should be understood as a sum over σ, an integration over the direction of $\mathbf{k}$, and an average over the initial states on the right hand side of equation (1). Note that hydrogen-like wave functions are more appropriate than planewaves in estimating w_{2f}, however, the analytic calculation becomes much more cumbersome [37]. One can show that the relative error of the planewave approximation is $\sim (L_m|\mathbf{k}_3|)^2$ [38], which is insignificant for carriers near the band extremes who have small momentums. For the annihilation of a free electron and a free hole, equation (1) is applicable to both direct and indirect transitions, and it will be used to calculate the recombination rate for the pathways (ii)–(iv).

For a direct band gap material, phonon assistance is not necessary for radiative recombination. In this case, $\mathbf{q} = 0$ and w_{2f} becomes w_{2f}^d [26] defined below:

$$w_{2f}^d = \frac{e^2}{V4\pi\epsilon_0} \frac{2\hbar\omega_{\mathbf{k}}}{m^2c^3} \Big|\frac{\epsilon_{\mathbf{k}\sigma\beta}k_{3\beta}}{\varepsilon(\omega_{\mathbf{k}})}\Big|^2. \quad (2)$$

For the annihilation of a free electron and a free hole, equation (2) will be used to estimate the ratio between the annihilation rate of an indirect transition and of a direct transition.

The recombination rate of the pathway (i) equals to the product of the formation probability of the mobile dying pair in a collision between two free carriers and the annihilation probability per unit time of the corresponding mobile dying pair. Noticing that in the collision of two free carriers, the annihilation takes place primarily for those wave-packets with $d_{eh} < L_m$, i.e. through a mobile dying pair. In other words, the recombination rate w_{2f} of the pathway (i) approximately equals to the annihilation rate of a mobile dying pair. Therefore, in the pathway (i), the formation probability of the dying pair is roughly unity; we can approximate the annihilation rate of the mobile dying pair by w_{2f}.

In the pathway (ii), two carriers are bound as an exciton. In this case, we can approximate the formation probability of the mobile dying pair as $V|\psi(0)|^2$, where $\psi(0)$ represents the wave-function of the electron at the position of the hole [39]. According to the hydrogenic model of excitons, $|\psi(0)|^2 = (\pi r_{ex}^3)^{-1}$, where $r_{ex} = \hbar(2m_{ex}E_{ex})^{-1/2}$ is the radius of the exciton; m_{ex} is the reduced mass of the electron and hole pair. Thus, the recombination rate in the pathway (ii) is $w_{ex} = V w_{2f}/(\pi r_{ex}^3)$.

The pathway (iii) involves the collision between a free carrier and a large polaron. To annihilate via this process, the electron (or hole) of the polaron must first break free from the surrounding lattice, facilitated by thermal activation or quantum tunneling. In this case, the free carrier and the polaron are in a bound state, and can be described by hydrogen-like wave-functions. The tunneling probability is the greatest if the free carrier is in contact with the polaron, i.e. the electron–hole distance is the radius of the polaron, R_P. Under this condition, the static Coulomb energy between them is $E'_{con} = Ke^2[R_P\varepsilon(0,T)]^{-1}$, where $\varepsilon(0,T)$ is the static dielectric function at temperature T. In contrast, the dynamic dielectric functions were used in equation (1). For electron–photon interaction, one requires dynamic dielectric function $\varepsilon(\omega_{\mathbf{k}})$ defined at the PL frequency of $\omega_{\mathbf{k}}$. For electron–phonon interaction, one needs $\varepsilon(\omega_{\mathbf{q}}^g)$ defined at the phonon frequency $\omega_{\mathbf{q}}^g$. Thus the probability of forming this contacting configuration is $p'_{con} = (e^{E'_{con}/k_BT} - 1)/(e^{E'_{con}/k_BT} + 1)$. By means of the molecular orbital theory, we can derive the probability (P'_{tun}) of an electron from the polaron tunneling to the nearby hole as:

$$P'_{tun} = \frac{R_P}{L_m}\left[\frac{2Ke^2}{R_P(B_m - E_P)\varepsilon}\right]^2 e^{-R_P/L_m}, \qquad (3)$$

where E_P is the formation energy of the polaron. Hence the formation probability of the mobile dying pair via tunneling is $P'_{tun}p'_{con}$. The same electron in polaron can also escape from the surrounding lattice distortion via thermal activation, and the formation probability of the dying pair by thermal activation is $e^{-F_P/k_BT}[1 + e^{-F_P/k_BT}]^{-1}$, where F_P is the formation free energy of the polaron. Note that we have made distinction between the formation energy and formation free energy of large polarons [7].

Super radiance transitions have been observed in halide perovskites and are important in charge recombination [40–42]. The transition moments of the mobile dying pairs formed by the tunneling are coherent [43, 44], while the transition moments of the dying pairs formed by the thermal activation are not coherent. Thus, the recombination rate w_{Pf} for the pathway (iii) is:

$$w_{Pf} = \left[P'_{tun}p'_{con}P'_{coh}C' + \frac{e^{-F_P/k_BT}}{1 + e^{-F_P/k_BT}}\right]w_{2f}, \qquad (4)$$

where P'_{coh} and C' are two quantities related to the coherent transitions and their expressions are given in the supplemental material (stacks.iop.org/JPhysCM/31/165701/mmedia).

Similarly, one can find the recombination rate along the pathway (iv) involving the collision of two polarons. The
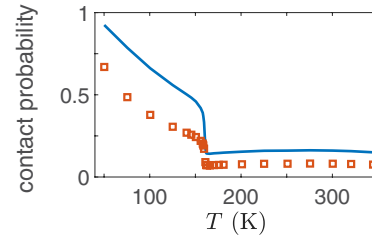

Figure 4. The contact probability $p'_{con}(T)$ between a free carrier and a polaron (solid line) and the contact probability $p_{con}(T)$ between two polarons in MAPbI₃. Parameters used in the calculations include $R_P = 28.3$ Å taken from [7] and $\varepsilon(0,T)$ taken from figure 3 of [21] and extrapolated to below 50K and above 345 K.

attraction energy E_{con} between two contacting polarons is $E_{con} = Ke^2[2R_P\varepsilon(0,T)]^{-1}$. At temperature T, the contact probability is $p_{con} = (e^{E_{con}/k_BT} - 1)/(e^{E_{con}/k_BT} + 1)$. The tunneling probability P_{tun} is:

$$P_{tun} = \frac{4e^{-2R_P/L_m}}{L_m R_P}\frac{(Ke^2/\varepsilon)^2}{[B_m - E_P]^2}. \qquad (5)$$

The formation probability of mobile dying pair through thermal activation is given by $e^{-2F_P/k_BT}[1 + e^{-2F_P/k_BT}]$. Thus the recombination rate along the pathway (iv) is:

$$w_{2P} = \left[P_{tun}p_{con}P_{coh}C + \frac{e^{-2F_P/k_BT}}{1 + e^{-2F_P/k_BT}}\right]w_{2f}. \qquad (6)$$

The expressions of P_{coh} and C are given in the supplemental material.

In figure 4, $p'_{con}(T)$ and $p_{con}(T)$ are plotted for MAPbI₃. In the calculations, $R_P = 28$ Å [7], $\varepsilon(0,T)$ is taken from [21]. One can see that the contact probability $p'_{con}(T)$ between a free carrier and a polaron and the contact probability $p_{con}(T)$ between two polarons decrease significantly with temperature, thus the tunneling and coherent radiation are only important below 150K.

We next turn to the immobile dying pair which is present in the pathways (v) and (vi). Let us first consider the annihilation between a free electron (or hole) and a trapped hole (or electron). To make the problem tractable, we approximate the wave-function of the trapped hole as $\chi_h = \pi^{-1/2}a_0^{-3/2}e^{-r/a_0}$, where $a_0 = 4\pi\epsilon_0\varepsilon_\infty\hbar^2/(mz_te^2)$ is the Bohr radius of the hole, and z_t is the effective nuclear charge of the trap. We can show that the annihilation rate w_{ft} between the free electron and the trapped hole is [37, 39]:

$$w_{ft} = \frac{\hbar\omega e^2}{V2\pi m^2c^3\epsilon_0}\left|\int\frac{d^3k_2}{(2\pi)^3}\frac{ik_{2\beta}}{\pi^{1/2}a_0^{3/2}}\right.$$

$$\left.\frac{2}{a_0[(\frac{1}{a_0})^2 + k_2^2]^2}\frac{z_te^2}{(E_{c\mathbf{k}_2} - E_{c\mathbf{k}_1})\varepsilon_\infty\epsilon_0|\mathbf{k}_2 - \mathbf{k}_1|^2}\right|^2, \qquad (7)$$

where $\mathbf{k}_1$ is the wave vector of the free electron, and ω is the photon frequency. Here w_{ft} should be understood as an average over various initial states on the right hand side of equation (7). Similar to the mobile dying pair, we can take w_{ft} as the annihilation rate for the immobile dying pair.
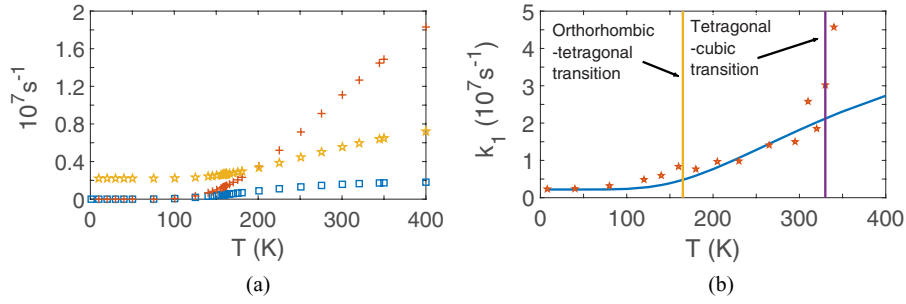
Figure 5. (a) Three contributions to k_1: exciton (squares), free carrier-trapped carrier (crosses) and polaron-trapped carrier (pentagons); (b) comparison of measured k_1 (pentagons) [52] with equation (9). The small nonzero values of k_1 below 150 K come from the annihilation between polaron and trapped carrier.

Finally, we consider the pathway (vi) involving the collision between a free polaron and a trapped carrier. In the collision of electron (hole) polaron with a trapped hole (electron), the electron (or hole) could escape from the surrounding lattice through tunneling to a close range of the trapped hole (electron). Neglecting the existence of trapping center, the contact probability between a polaron and a trapped carrier is determined by p'_{con}, the tunneling probability of electron (hole) from surrounding lattice is P'_{tun}. The escape of electron (hole) from electronic (hole) polaron can also occur by thermal activation, the formation probability of immobile dying pair through thermal activation is $e^{-F_P/k_BT}[1 + e^{-F_P/k_BT}]^{-1}$. Thus, the recombination rate along pathway (vi) is

$$w_{Pt} = \left(P'_{tun}p'_{con} + \frac{e^{-F_P/k_BT}}{1 + e^{-F_P/k_BT}}\right)w_{ft}. \tag{8}$$

For MAPbI$_3$, the relevant materials parameters $E_P = 70$ meV, $F_P = 40$–70 meV [7], $E_{tra} = 0.2$ eV [32]. $\varepsilon(0, T)$ is taken from [21]. L_m and B_m are obtained earlier. Using these parameters, and equations (4), (6) and (8), we find that the recombination rates of the polarons (w_{Pf}, w_{2P}, w_{Pt}) are 2–3 orders of magnitude slower than those of free carriers (w_{2f}, w_{ft}).

Assuming all photo-generated carriers existed as free carriers, the slow charge recombination in OIHPs has also been explained by the formation of an indirect band gap originated from the spin–orbit coupling [45–49] and/or ionic lattice distortion [50, 51]. Let q denote the relative shift between the bottom of the conduction band and the top of the valence band in the reciprocal space, and it has been shown that $|q| < 0.1$ Å $\ll \pi/a$ [45–51]. Using equations (1) and (2), one can estimate that $w_{2f}/w_{2f}^d \approx 0.1$–$0.3$. This suggests if the charge carriers are 'free' electrons and holes as opposed to large polarons, their recombination rates would be slowed down by a factor of 3–10, owing to the shift of the band gap. This factor is much smaller than that (10^2–10^3) induced by the formation of large polarons.

5. Monomolecular and bimolecular recombination rates

As an important tool to examine light-matter interactions, PL is widely used to characterize radiative recombination in OIHPs. Charge recombination in a semiconductor can be described

by the following equation: $dn_e/dt = -k_1n_e - k_2n_e^2 - k_3n_e^3$ [52, 53], where n_e is the electron density; k_1 is the monomolecular charge recombination rate, k_2 is the bimolecular charge recombination rate and k_3 is the Auger charge recombination rate. Since Auger recombination is generally much weaker compared to the other two at the normal operating conditions, here we focus on k_1 and k_2. According to our theory, the following one-body pathways contribute to the monomolecular recombination rate k_1: (ii) annihilation of electron and hole of an exciton; (v) annihilation of a free carrier and a trapped carrier, and (vi) annihilation of a polaron and a trapped carrier. Hence we have

$$k_1 = p_{ex}w_{ex} + 2p_{ft}(Vn_tw_{ft}) + 2p_{Pt}(Vn_tw_{Pt}), \tag{9}$$

where n_t is the density of the traps. The bimolecular recombination rate k_2 consists of following contributions: annihilation between two free carriers (i), between two polarons (iv), and between a free carrier and a polaron (iii). Thus we have

$$k_2 = p_{2P}(Vw_{2P}) + 2p_{Pf}(Vw_{Pf}) + p_{2f}(Vw_{2f}). \tag{10}$$

To validate our microscopic theory, we apply equations (9) and (10) to calculate k_1 and k_2 of MAPbI$_3$ for which many experimental results are available. Here we take the following materials parameters from experiments although some of them can also be calculated from first-principles. More specifically, $E_P = 70$ meV [7], $r_{ex} = 49$ Å, $m_{ex} = 0.1$ m [33], $z_t = 1$, $n_t = 3 \times 10^{10}$ cm^{-3} [30]. The dielectric function $\varepsilon(0, T)$ is measured for 50 K $< T <$ 345 K [21], while k_1 and k_2 are measured for 8 K $< T <$ 370 K [52]. We extrapolate the experimental $\varepsilon(0, T)$ value to below 50 K and above 345 K.

In figure 5(a), three contributions to k_1 are plotted. At low temperature, the percentages of excitons and free carriers are very small (see figure 1), and polarons are dominant carriers. Therefore below 150 K, the small monomolecular annihilation rate comes from the immobile dying pairs formed through tunneling in the collisions of polarons and trapped carriers (pathway (vi)); the pathways (ii) and (v) make no appreciable contribution to k_1. Above 150 K, all three pathways (ii), (v) and (vi) have significant contributions.

In figure 6, three contributions to k_2 are plotted. Below 150K, the annihilation between two polarons (pathway (iv)) is the most important. Above 150 K, the pathways (iii) and (i) are more important. The sudden increase of the dielectric function $\varepsilon(0, T)$ around 150 K [21] leads to a drastic decrease
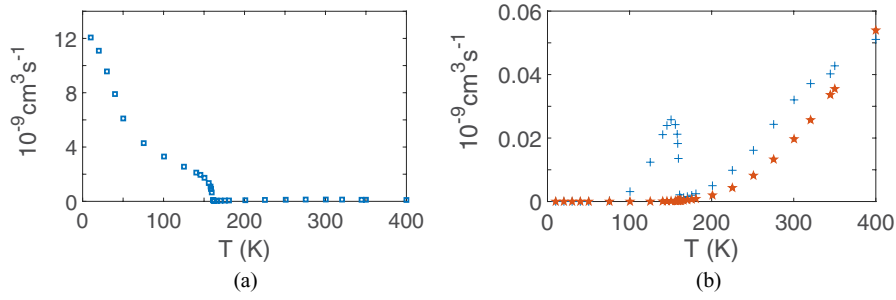
Figure 6. (a) Contribution to k_2 from the annihilation of two polarons (squares). (b) Contributions to k_2 from the annihilation of polaron-free carrier (crosses), and the annihilation of free electron and free hole (pentagons).

in the contact probabilities $p_{con}(T)$ and $p'_{con}(T)$, consequently, an abrupt decrease of the annihilation rates in the pathways (iv) and (iii).

Since the experiment of Milot *et al* [52] is the only one that systematically measured k_1 and k_2 as a function of temperature, to the best of our knowledge, we compare our theoretical values to their experimental data in figure 5(b) for k_1 and figure 7 for $Log_{10}(k_2)$, where w_{2f} and w_{ft} are used as two fitting parameters. Generally, there are good agreements between the theory and the experiment for a wide range of temperatures. However, some discrepancies are evident, specially around the two known structural phase transitions at 155 K and 330 K. The theory reproduces the general experimental trends that k_1 increases monotonically while k_2 decreases first and then increases with increasing temperature.

The apparent discrepancies between the theory and experimental values of k_2 around 310 K may be attributed to strong ferroelectric fluctuation [54, 55] which could separate the positive and negative charges across the domains, leading to a sharp decrease of k_2 around 310 K. On the other hand, the sudden rise of k_2 at 310 K may be due to the fact that at higher temperatures, the electrons are too fast for the lattice deformation to follow [7, 56], and thus the carriers can escape from the surrounding lattice without resorting to tunneling or thermal activation. In the present framework, we did not take into account this mechanism.

6. Peak and width of PL spectra

We can estimate the PL peak frequency (ω_{PL}) as a function of the incident flux I and temperature T. According to the polaron theory [20], the formation energy E_P of a large polaron is determined by

$$E_P(T) = \frac{V_L^2}{4T_e},\tag{11}$$

where

$$T_e = \frac{\hbar^2}{2mr^2}\tag{12}$$

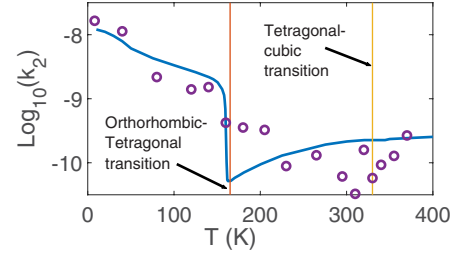is the kinetic energy of an electron in the conduction band, m is the mass of electron.

Figure 7. The logarithm of the bimolecular recombination rate k_2 (cm^3 s^{-1}) as a function of temperature in MAPbI$_3$: solid curve is calculated from equation (10) and the experimental values (circles) are taken from [52].

$$V_L(T) = \frac{1}{4\pi\epsilon_0}\frac{e^2}{2}[\frac{1}{\varepsilon_\infty} - \frac{1}{\varepsilon(0,T)}]\frac{1}{r},\tag{13}$$

is the coupling between the electron and the optical phonon, r is the characteristic length which the electron wavefunction changes significantly. For CH$_3$NH$_3$PbI$_3$ lattice constant $a = 6.3$ Å [57], $\varepsilon(0, 300$ K$) = 70$, and $\varepsilon_\infty = 6.5$ [34]. If we take r as the Pb–I bond length $\sim$3 Å , then $T_e \sim 0.42$ eV, $V_L \sim 0.33$ eV, $E_P(300$ K$) \sim 66.6$ meV. From $E_P(T)$, one can calculate the formation free energy $F_P(T)$ of polaron [7].

Since large polarons are dominant carriers in OIHPs under normal conditions, the PL spectrum is primarily determined by polaron recombination. Thus, ω_{PL} can be approximated by the energy difference between an EP and a HP, which have the highest density of states. Specifically, the most populated EP energy level can be written as $c_b + g - F_P(T)$, where c_b is the bottom of the conduction band. g is the chemical potential of polaron gas at temperature T, given by $g = \varepsilon_F[1 - (\pi k_B T/2\varepsilon_F)^2/3]$. ε_F is the Fermi energy of the polaron gas and $\varepsilon_F = \hbar^2(3\pi^2 n_e)^{2/3}/2m_P$. Here $n_e = I\phi[\varepsilon(\omega)]^{1/2}/c$ is the number density of incident photons, ω is the excitation frequency, c is the speed of light in vacuum, I is the incident photon flux [31]. We assume the quantum yield efficiency $\phi = 1$ [31], $\varepsilon(\omega) \approx 6.5$ [34], then n_e is the concentration of photon-generated electrons. Since the percentage of polarons is much larger than that of excitons and free carriers, n_e is approximately the concentration of polarons. Similarly, the most populated HP energy level
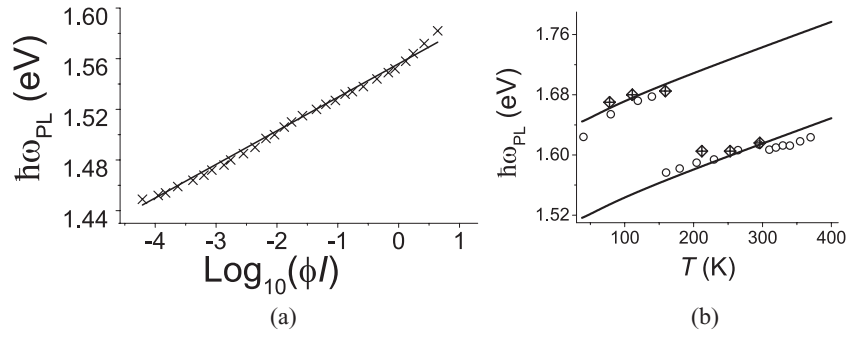
Figure 8. (a) PL peak frequency ω_{PL} of MAPbI$_3$ as a function of the incident flux I: the experimental data (cross) is taken from [59] and the solid line is calculated from equation (14). To simplify the calculation we take $\phi = 1$ for all incident flux. (b) ω_{PL} of MAPbI$_3$ as a function of temperature: the solid lines are calculated from equation (14) and the experimental values (circles) are taken from [52], and (diamonds) taken from [48]. The upper curve is for low temperature orthorhombic phase and the lower curve is for higher temperature tetragonal phase.

can be written as $v_t - g + F_P(T)$, with v_t being the top of the valence band. Therefore, we arrive at

$$\hbar\omega_{PL}(T) = (c_b - v_t) - 2F_P(T)$$

$$+ 2\varepsilon_F[1 - \frac{1}{3}(\frac{\pi k_B T}{2\varepsilon_F})^2]. \quad (14)$$

In figure 8(a), we plot $\omega_{PL}(I)$ as a function of incident light flux I for MAPbI$_3$, which is measured at room temperature $T = 300$ K. For MAPbI$_3$, $m_P = 4.1$ m [7] and $\varepsilon(\omega) = 6.5$ [34]. The agreement with the experimental data is very good. Furthermore, temperature dependence of $\omega_{PL}(T)$ has also been reported for MAPbI$_3$ [48, 52, 58]. The two solid lines in figure 8(b) are computed for $n_e = 10^{17}$ cm^{-3}. Once again, our theoretical calculations compare very well to the experimental measurements, as shown in figure 8(b). The upper curve is for the low temperature orthorhombic phase while the lower curve is for the higher temperature tetragonal phase. The two curves do not correspond to different flux.

Although polarons are dominant carriers in OIHPs, a model based on free carriers [60–62] yielded excellent fits to the experimental line width. In fact, the model appeared to work very well for four different halide perovskites [62]. This apparent contradiction can be explained by our theory. It is known that the line width of a PL spectrum is determined by the energy uncertainty of the recombination processes. Along each of the recombination pathways, the electron and hole of a dying pair are no longer confined by its surrounding lattice. According to the annihilation rate w_{2f}, we find that the recombination time of the mobile dying pair is in the order of 10^{-9} s, which is much larger than the timescale ($\sim10^{-13}$ s) of absorbing and emitting LO phonons [6, 63]. In other words, the coupling of the 'free' electron (or hole) with LO phonons is the dominant process for determining the line width.

The polaron pairs do not directly lead to the PL spectrum, but rather proceed via the formation of the mobile dying pairs. In other words, the PL peak width is entirely determined by the contribution of the mobile dying pairs. In the normal operation condition, the concentration of photo-generated carriers is in the range of 10^{13}–10^{18} cm^{-3}. Because the concentration of traps is small: $n_t = 3 \times 10^{10}$ cm^{-3} [30], and the percentages of excitons and of free carriers are much smaller than that of polarons (see figure 1), one can see from equations (9)

and (10) that the rate of the monomolecular recombination is much slower than the rate of the bimolecular recombination. Thus, the PL mainly comes from the bimolecular recombination [52, 62]. All three pathways (i), (iii) and (iv) for k_2 pass through the mobile dying pairs. The line width of PL spectrum is determined by the interaction of 'free' electron (or hole) in the mobile dying pairs with LO phonons; this is consistent with the previous model [60–62] which calculated the PL line width based on the interaction of free carriers with LO phonons.

7. Conclusion

In conclusion, we proposed a microscopic theory for radiative recombination of large polarons in OIHPs. Six relevant recombination pathways are identified and their statistical weights are estimated for MAPbI$_3$. Radiative recombination proceeds via dying pairs along each pathway. There are two types of dying pairs—mobile and immobile—which are responsible for charge recombination. The formation probability of the dying pair along each pathway can be determined and the annihilation rate of each dying pair can be estimated. The product of the formation probability and the annihilate rate gives rise to the recombination rate along each pathway and the weighted sum of the recombination rates yields the overall rate of radiative recombination in OIHPs. Applying the theory to MAPbI$_3$, we can evaluate the monomolecular and bimolecular recombination rates, k_1 and k_2 of PL spectrum as a function of temperature, and its peak frequency as a function of incident light flux and temperature. In general, good agreements between the theory and experiments are obtained, providing a validation of the theory. Finally, we explain why a simple model based on free electrons and holes could be sufficient to reproduce the experimental PL line width. Our work elucidates the microscopic mechanism by which large polarons recombine in OIHPs via the formation of the dying pairs assisted by thermal activation and quantum tunneling.

Acknowledgments

ORCID iDs

Mingliang Zhang ⬤ https://orcid.org/0000-0002-9959-8502
Xu Zhang ⬤ https://orcid.org/0000-0002-6491-3234

References

[1] Huang J, Yuan Y, Shao Y and Yan Y 2017 *Nat. Rev. Mater.* **2** 17042
[2] Sutherland B R and Sargent E H 2016 *Nat. Photon.* **10** 295302
[3] Brenner T M, Egger D A, Kronik L, Hodes G and Cahen D 2016 *Nat. Rev. Mater.* **1** 15007
[4] Zhu X Y and Podzorov V 2015 *J. Phys. Chem. Lett.* **6** 4758
[5] Brenner T M, Egger D A, Rappe A M, Kronik L, Hodes G and Cahen D 2015 *J. Phys. Chem. Lett.* **6** 4754
[6] Zhu H, Miyata K, Fu Y, Wang J, Joshi P P, Niesner D, Williams K W, Jin S and Zhu X Y 2016 *Science* **353** 1409
[7] Zhang M, Zhang X, Huang L Y, Lin H Q and Lu G 2017 *Phys. Rev.* B **96** 195203
[8] Bonn M, Miyata K, Hendry E and Zhu X Y 2017 *ACS Energy Lett.* **2** 2555
[9] Menendez-Proupin E, Palacios P, Wahnon P and Conesa J C 2014 *Phys. Rev.* B **90** 045207
[10] Sendner M *et al* 2016 *Mater. Horiz.* **3** 613
[11] Frost J M, Butler K T and Walsh A 2014 *APL Mater.* **2** 081506
[12] Frost J M 2017 *Phys. Rev.* B **96** 195202
[13] Frost J M, Whalley L D and Walsh A 2017 *ACS Energy Lett.* **2** 2647
[14] Evans T J S, Miyata K, Joshi P P, Maehrlein S, Liu F and Zhu X Y *J. Phys. Chem.* C **122** 13724–30
[15] Eglitis R, Kotomin E, Borstel G, Kapphan S and Vikhnin V 2003 *Comput. Mater. Sci.* **27** 81
[16] Eglitis R I 2014 *Int. J. Mod. Phys.* B **28** 1430009
[17] Wang C, Ecker B R, Wei H, Huang J, Meng J Q and Gao Y 2017 *Phys. Chem. Chem. Phys.* **19** 5361
[18] Niesner D, Wilhelm M, Levchuk I, Osvet A, Shrestha S, Batentschuk M, Brabec C and Fauster T 2016 *Phys. Rev. Lett.* **117** 126401
[19] Lee M I *et al* 2017 *J. Phys. D: Appl. Phys.* **50** 26LT02
[20] Emin D 2013 *Polarons* (Cambridge: Cambridge University Press)
[21] Onoda-Yamamuro N, Matsuo T and Suga H 1992 *J. Phys. Chem. Solids* **53** 935
[22] Brivio F, Butler K T, Walsh A and van Schilfgaarde M 2014 *Phys. Rev.* B **89** 155204
[23] Miyata K, Meggiolaro D, Trinh M T, Joshi P P, Mosconi E, Jones S C, De Angelis F and Zhu X Y 2017 *Sci. Adv.* **3** e1701217
[24] Emin D 2018 *J. Appl. Phys.* **123** 055105
[25] Munson K T, Kennehan E R, Doucette G S and Asbury J B 2018 *Chem* **4** 2826–43
[26] Bethe H A and Salpeter E E 2014 *Quantum Mechanics of One- And Two-Electron Atoms* (Eastford: Martino Fine Books)
[27] Joshi B 2015 *Discrete Continuous Dyn. Syst. Ser.* B **20** 1077
[28] Gorban A 2014 *Results Phys.* **4** 142
[29] Dong Q, Fang Y, Shao Y, Mulligan P, Qiu J, Cao L and Huang J 2015 *Science* **347** 967
[30] Shi D *et al* 2015 *Science* **347** 519
[31] Oga H, Saeki A, Ogomi Y, Hayase S and Seki S 2014 *J. Am. Chem. Soc.* **136** 13818
[32] Yin W J, Shi T and Yan Y 2015 *J. Phys. Chem.* C **119** 5253
[33] Miyata A, Mitioglu A, Plochocka P, Portugall O, Wang J T W, Stranks S D, Snaith H J and Nicholas R J 2015 *Nat. Phys.* **11** 582
[34] Lin Q, Armin A, Nagiri R C R, Burn P L and Meredith P 2015 *Nat. Photon.* **9** 106
[35] Dumke W P 1957 *Phys. Rev.* **105** 139
[36] Schlangenotto H, Maeder H and Gerlach W 1974 *Phys. Status Solidi* a **21** 357
[37] Jauch J M and Rohrlich F 1980 *Theory of Photons and Electrons* 2nd edn (Berlin: Springer)
[38] Schiff L I 1968 *Quantum Mechanics* 3rd edn (New York: Mcgraw-Hill)
[39] Berestetski V B, Lifshitz E M and Pitaevskii L P 1982 *Quantum Electrodynamics* 2nd edn (Oxford: Pergamon)
[40] Priante D, Dursun I, Alias M S, Shi D, Melnikov V A, Ng T K, Mohammed O F, Bakr O M and Ooi B S 2015 *Appl. Phys. Lett.* **106** 081902
[41] Raino G, Becker M A, Bodnarchuk M I, Mahrt R F, Kovalenko M V and Stferle T 2018 *Nature* **563** 671
[42] Sum T C and Mathews N 2019 *Halide Perovskites: Photovoltaics, Light Emitting Devices, and Beyond* (New York: Wiley)
[43] Dicke R H 1954 *Phys. Rev.* **93** 99
[44] Gross M and Haroche S 1982 *Phys. Rep.* **93** 301
[45] Azarhoosh P, McKechnie S, Frost J M, Walsh A and van Schilfgaarde M 2016 *APL Mater.* **4** 091501
[46] Etienne T, Mosconi E and De Angelis F 2016 *J. Phys. Chem. Lett.* **7** 1638
[47] Wang T, Daiber B, Frost J M, Mann S A, Garnett E C, Walsh A and Ehrler B 2017 *Energy Environ. Sci.* **10** 509
[48] Even J, Pedesseau L and Katan C 2014 *J. Phys. Chem.* C **118** 11566
[49] Kepenekian M, Robles R, Katan C, Sapori D, Pedesseau L and Even J 2015 *ACS Nano* **9** 11557
[50] Motta C, El-Mellouhi F, Kais S, Tabet N, Alharbi F and Sanvito S 2015 *Nat. Commun.* **6** 7026
[51] Zhang X, Zhang M and Lu G 2016 *J. Phys. Chem.* C **120** 23969
[52] Milot R L, Eperon G E, Snaith H J, Johnston M B and Herz L M 2015 *Adv. Funct. Mater.* **25** 6218
[53] Savenije T J *et al* 2014 *J. Phys. Chem. Lett.* **5** 2189
[54] Liu S, Zheng F, Koocher N Z, Takenaka H, Wang F and Rappe A M 2015 *J. Phys. Chem. Lett.* **6** 693
[55] Rakita Y, Bar-Elli O, Meirzadeh E, Kaslasi H, Peleg Y, Hodes G, Lubomirsky I, Oron D, Ehre D and Cahen D 2017 *Proc. Natl Acad. Sci. USA* **114** E5504
[56] Davydov A S and Enolskii V Z 1987 *Phys. Status Solidi* b **143** 167
[57] Brivio F, Walker A B and Walsh A 2013 *APL Mater.* **1** 042111
[58] Foley B J, Marlowe D L, Sun K, Saidi W A, Scudiero L, Gupta M C and Choi J J 2015 *Appl. Phys. Lett.* **106** 243904
[59] Dar M I, Jacopin G, Meloni S, Mattoni A, Arora N, Boziki A, Zakeeruddin S M, Rothlisberger U and Grätzel M 2016 *Sci. Adv.* **2** e1601156
[60] Lee J, Koteles E S and Vassell M O 1986 *Phys. Rev.* B **33** 5512
[61] Rudin S and Reinecke T L 1990 *Phys. Rev.* B **41** 3017
[62] Wright A D, Verdi C, Milot R L, Eperon G E, Perez-Osorio M A, Snaith H J, Giustino F, Johnston M B and Herz L M 2016 *Nat. Commun.* **7** 11755
[63] Yang Y, Ostrowski D P, France R M, Zhu K, van de Lagemaat J, Luther J M and Beard M C 2015 *Nat. Photon.* **10** 53